

Transport by bi-harmonic drives: from harmonic to vibrational mixing

M. Borromeo, Peter Hänggi, Fabio Marchesoni

Angaben zur Veröffentlichung / Publication details:

Borromeo, M., Peter Hänggi, and Fabio Marchesoni. 2005. "Transport by bi-harmonic drives: from harmonic to vibrational mixing." *Journal of Physics: Condensed Matter* 17 (47): S3709–18. <https://doi.org/10.1088/0953-8984/17/47/005>.



Transport by bi-harmonic drives: from harmonic to vibrational mixing

M Borromeo^{1,2}, P Hänggi³ and F Marchesoni⁴

¹ Dipartimento di Fisica, Università di Perugia, I-06123 Perugia, Italy

² Istituto Nazionale di Fisica Nucleare, Sezione di Perugia, I-06123 Perugia, Italy

³ Institute of Physics, University of Augsburg, Universitätsstrasse 1, D-86135 Augsburg, Germany

⁴ Dipartimento di Fisica, Università di Camerino, I-62032 Camerino, Italy

Abstract

Transport in a one-dimensional symmetric device can be activated by the combination of thermal noise and a bi-harmonic drive. The results of extensive simulations allow us to distinguish between two apparently different bi-harmonic regimes: (i) *harmonic mixing*, where the two drive frequencies are commensurate but not too high; (ii) *vibrational mixing*, where one harmonic drive component possesses a high frequency but finite amplitude-to-frequency ratio. A comparison with the earlier theoretical predictions shows that at present the analytical understanding of nonlinear frequency mixing is still not satisfactory.

1. Introduction

We know from the literature of the 1970s [1] that a charged particle confined onto a nonlinear substrate is capable of mixing two alternating input electric fields of angular frequencies Ω_1 and Ω_2 ; its response is expected to contain all possible harmonics of Ω_1 and Ω_2 . As a result, for commensurate input frequencies, i.e., $m\Omega_1 = n\Omega_2$, the time-dependent particle velocity generally (i.e. if not forbidden by reasons of symmetry) would contain a dc component, too. Such a phenomenon, termed in the later literature *harmonic mixing* (HM), is a rectification effect induced by the asymmetry of the applied force [2]. In view of general perturbation arguments, HM was predicted to be of the $(n + m)$ th order in the dynamical parameters of the system [3–5]. Recently, HM was re-interpreted as a manifestation of the Brownian motor phenomenon [6], even if no spatial asymmetry of the substrate is required to generate an HM signal [6–8]. The extension of HM to Hamiltonian systems also resulted in interesting applications [9].

More recently, the HM mechanism has been investigated numerically as a tool to control the transport of interacting particles in artificially engineered quasi-one-dimensional

channels [10, 11]. An interesting variation of this problem has been proposed in the context of soliton dynamics, where the combination of two ac driving forces was proven to rectify the motion of a kink-bearing chain owing to the inherent nonlinearity of the travelling kinks [12].

Here, we study a Brownian particle moving on a one-dimensional substrate subjected to an external bi-harmonic force $F(t)$ and a zero-mean valued, delta-correlated Gaussian noise $\xi(t)$. Its coordinate $x(t)$ obeys the Langevin equation (LE)

$$\dot{x} = -V'(x) + F(t) + \xi(t), \quad (1)$$

where $\langle \xi(t) \rangle = 0$, $\langle \xi(t)\xi(0) \rangle = 2D\delta(t)$,

$$F(t) = A_1 \cos(\Omega_1 t + \phi_1) + A_2 \cos(\Omega_2 t + \phi_2) \quad (2)$$

with $A_1, A_2 \geq 0$, and $V(x)$ being the periodic substrate potential with period $L = 2\pi$ defined by

$$V(x) = \sum_{n=1}^{\infty} a_n \cos(nx) + \sum_{n=1}^{\infty} b_n \sin(nx), \quad (3)$$

for an appropriate choice of the Fourier coefficients $\{a_n\}$ and $\{b_n\}$.

In this report we compare the results of extensive numerical simulations with the perturbation predictions for the rectification current $\langle \dot{x} \rangle / 2\pi$ induced by HM. We conclude that, in spite of the abundance of numerical results, the analytical description of HM available in the literature is still not complete, and is to some extent not even satisfactory. Additionally, we explore a new nonlinear mixing regime. We assume that a weak input signal is tuned at an optimal frequency Ω_1 that maximizes the particle response, whereas a high-frequency perturbation pumps energy into the system forcing free particle oscillations of amplitude $\psi_0 = A_2/\Omega_2$ comparable with the system length-scale; the ratio Ω_2/Ω_1 , not necessarily a rational number, can be several orders of magnitude large. We demonstrate that the particle response at the low frequency Ω_1 is extremely sensitive to the high-frequency pump parameter ψ_0 , thus suggesting a totally new frequency mixing mechanism, termed here *vibrational mixing* (VM) [14].

2. Harmonic mixing

Let us start with the simplest case possible, namely the overdamped stochastic dynamics (1) driven by the bi-harmonic force (2) with $\phi_1 = \phi_2$ and $\Omega_2 = 2\Omega_1$, on the substrate with potential

$$V(x) = d(1 - \cos x). \quad (4)$$

A truncated continued fraction expansion [3] led to the conclusion that in the regime of low temperature, $D \ll d$, the non-vanishing dc component $\langle \dot{x} \rangle$ of the particle velocity would scale like

$$\frac{\langle \dot{x} \rangle}{D} \propto - \left(\frac{A_1}{2D} \right)^2 \frac{A_2}{2D}. \quad (5)$$

This result suggests that for small drive amplitudes and high substrate barriers, $A_1, A_2 \ll D \ll d$, the HM signal is *negative* and independent of d , at variance with the numerical results reported in figure 1. Numerical simulation runs for increasing d -values reveal a resonant $\langle \dot{x}(d) \rangle$ curve. This is no surprise, as for $d \rightarrow 0$ (flattening substrate) the unbiased, zero-mean force (2), with $\langle F(t) \rangle = 0$, cannot sustain a non-null drift current, whereas for $d \rightarrow \infty$ (high substrate barriers) the interwell activation mechanism gets exponentially suppressed and the

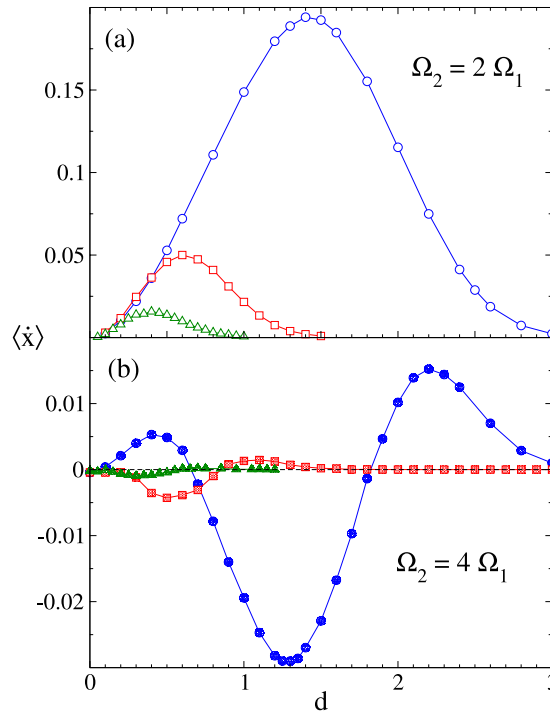


Figure 1. Transport via HM in the cosine potential (4) for $\phi_1 = \phi_2$, $A_1 = A_2$, and (a) $\Omega_2 = 2\Omega_1$, (b) $\Omega_2 = 4\Omega_1$: $\langle \dot{x} \rangle$ versus d . Simulation parameters: $\Omega_1 = 0.01$, $D = 0.2$, and $A_1 = 0.2$ (triangles), $A_1 = 0.4$ (squares), and $A_1 = 1.1$ (circles).

relevant drift current drops to zero. (The conflicting sign in equation (5) is likely to be due to an erroneous definition in [3].)

The numerical dependence of $\langle \dot{x} \rangle$ on the amplitude of $F(t)$ is also more complicated than expected from the perturbation estimate (5). In figure 2, the HM dc component of $\dot{x}(t)$ is plotted versus $A_1 = A_2 \equiv A$ at different drive frequencies $\Omega_2 = 2\Omega_1$. For low drive amplitudes the HM signal $\langle \dot{x} \rangle$ indeed grows proportionally to A^3 as suggested by the scaling law (5), but only for sufficiently high noise level D .

Moreover, figure 2 illustrates another interesting property of rectification by HM: at relatively high ac frequencies (non-adiabatic regime), the curves $\langle \dot{x}(A) \rangle$ develop regular oscillations for $A > 1$ with period and amplitude roughly proportional to Ω_1 . The details of such a non-adiabatic mechanism are explained in [13]: on setting A at increasingly high values above the depinning threshold of $V(x)$, $\max\{|V'(x)|\} = 1$, it happens that the number of substrate cells the driven particle drifts across during one half-cycle increases by one unit, first to the right and then to the left, thus causing one full $\langle \dot{x} \rangle$ oscillation at regular A increments, ΔA , proportional to Ω_1 . Of course, in the adiabatic limit, $\Omega_1 \rightarrow 0$, these oscillations tend to disappear with ΔA . Moreover, shortening the drive period or lowering the noise level for $A > 1$ enhances the above modulation effect [13]. Finally, on further increasing A the cancellation of the right and the left drifts becomes more and more efficient; as a result the envelope of the $\langle \dot{x} \rangle$ oscillations decays slowly with A —seemingly, inversely proportionally to \sqrt{A} (see figure 2).

An independent perturbation approach [4] led to the following scaling law for the rectification velocity of a Brownian particle (1) in a cosine potential (4) subject to the harmonic

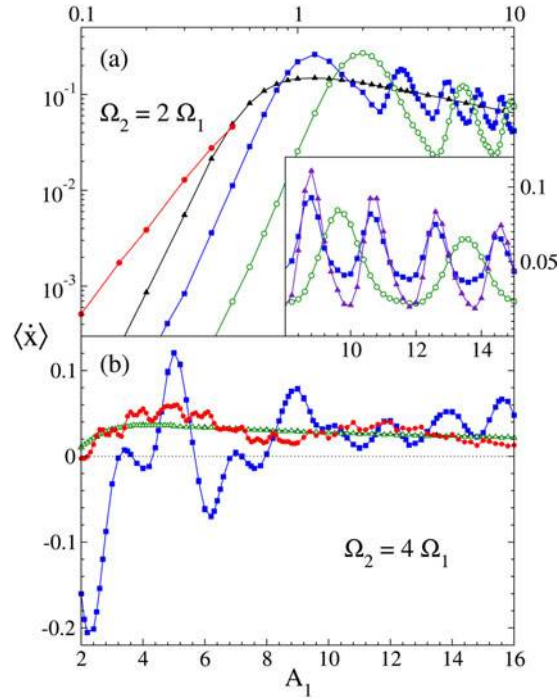


Figure 2. Transport via HM in the cosine potential (4) for $\phi_1 = \phi_2$, $A_1 = A_2$, and (a) $\Omega_2 = 2\Omega_1$, (b) $\Omega_2 = 4\Omega_1$: $\langle \dot{x} \rangle$ versus A_1 . Simulation parameters: (a) squares: $\Omega_1 = 0.4$, $D = 0.2$; empty circles: $\Omega_1 = 0.8$, $D = 0.2$; triangles: $\Omega_1 = 0.01$, $D = 0.2$; solid circles: $\Omega_1 = 0.05$, $D = 0.4$; (b) squares: $\Omega_1 = 0.4$, $D = 0.2$; circles: $\Omega_1 = 0.1$, $D = 0.2$; triangles: $\Omega_1 = 0.01$, $D = 0.2$. In both panels $d = 1$.

force (2) with $\Omega_2 = 2\Omega_1$:

$$\frac{\langle \dot{x} \rangle}{\Omega_1} \propto \left(\frac{d}{D} \right)^2 \left(\frac{A_1}{2\Omega_1} \right)^2 \frac{A_2}{2\Omega_2}. \quad (6)$$

This prediction, that applies under the conditions $d \ll \Omega_1 \ll D$, reproduces qualitatively only both the $d \rightarrow 0$ branches of figure 1 (consistently with [3]) and the $\Omega_1 \rightarrow \infty$ tails of the curves $\langle \dot{x}(\Omega_1) \rangle$ in figure 3. Note that for large commensurate drive frequencies, i.e., $\Omega_1 = m\Omega_0$ and $\Omega_2 = n\Omega_0$ with $\Omega_0 \rightarrow \infty$, the HM signal drops sharply to zero.

3. Vibrational mixing

In order to describe the VM mechanism in some detail, we now go back to equations (1)–(3) and further assume that one sinusoid of $F(t)$ is slow while the other one is fast, say, $\Omega_1 \ll \Omega_2$. Then, following the approach of [15, 16], we can separate

$$x(t) \longrightarrow x(t) + \psi(t), \quad (7)$$

where, in shorthand notation, from now on $x(t)$ represents a slowly time-modulated stochastic process and $\psi(t)$ is the particle free spatial oscillation

$$\psi(t) = \psi_0 \sin(\Omega_2 t + \phi_2) \quad (8)$$

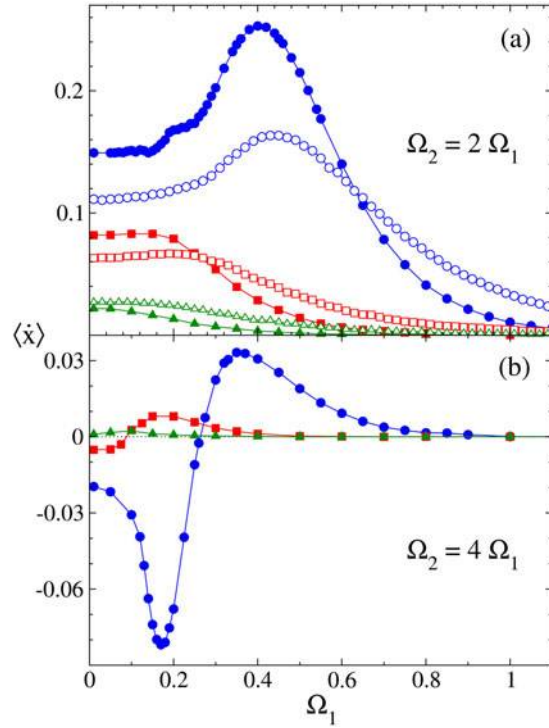


Figure 3. Transport via HM in the cosine potential (4) for $\phi_1 = \phi_2$, $A_1 = A_2$, and (a) $\Omega_2 = 2\Omega_1$, (b) $\Omega_2 = 4\Omega_1$: $\langle \dot{x} \rangle$ versus Ω_1 . Simulation parameters: solid symbols: $D = 0.2$; empty symbols: $D = 0.4$; triangles: $A_1 = 0.4$; squares: $A_1 = 0.6$; circles: $A_1 = 1.1$; in both panels $d = 1$.

with $\psi_0 = A_2/\Omega_2$. On averaging out $\psi(t)$ over time, the LE for the slow reduced spatial variable $x(t)$ can be written as [17]

$$\dot{x} = -V'(x) + A_1 \cos(\Omega_1 t + \phi_1) + \xi(t), \quad (9)$$

where

$$V(x) = \sum_{n=1}^{\infty} a_n J_0(n\psi_0) \cos(nx) + \sum_{n=1}^{\infty} b_n J_0(n\psi_0) \sin(nx). \quad (10)$$

Here, we made use of the identities $\langle \sin[n\psi(t)] \rangle = 0$ and $\langle \cos[n\psi(t)] \rangle = J_0(n\psi_0)$, with $J_0(x)$ denoting the Bessel function of 0-order [18]—see also inset of figure 4—and $\langle (\dots) \rangle$ representing the time average of the argument (\dots) .

As a result of the adiabatic elimination [19] of $\psi(t)$, the slow observable $x(t)$ diffuses on an effective or renormalized potential $V(x)$ driven by the slow harmonic of equation (2), alone. We remark that $V(x)$ depends on the ratio $\psi_0 = A_2/\Omega_2$, the amplitude of its n th Fourier component oscillating like $|J_0(n\psi_0)|$. The adiabatic separation (7) for $\Omega_1 \ll \Omega_2$ is tenable as long as the fast oscillation amplitudes are clearly distinguishable with respect to the corresponding Brownian diffusion [19], that is to say when $\psi_0^2 \gg 2Dt_2$ with $t_2 = 2\pi/\Omega_2$ or, equivalently,

$$D \ll \frac{A_2}{8\pi} \left(\frac{A_2}{\Omega_2} \right). \quad (11)$$

In the limit $\Omega_2 \rightarrow \infty$ at constant A_2/Ω_2 , the approximate LE (9) is expected to be very accurate, regardless of the value of D .

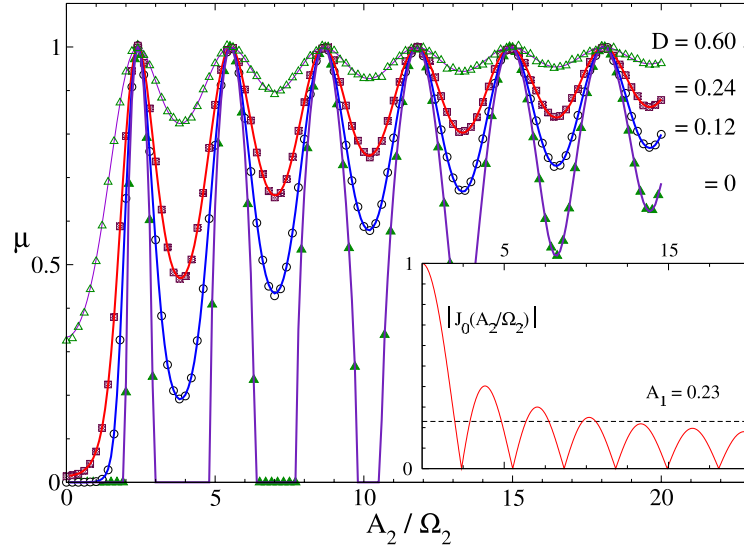


Figure 4. Mobility versus A_2/Ω_2 in the dc case, $\Omega_1 = 0$ and $\phi_1 = 0$, for different D . The simulation data (dots) have been obtained by integrating the LE (1) numerically with $V(x)$ given in equation (12) and parameter values $A_1 = 0.23$, $\Omega_2 = 0.1$. The solid curves represent the corresponding analytic prediction (11.51) of [20] for the reduced LE (9). Inset: amplitude $|J_0(A_2/\Omega_2)|$ of $\bar{V}(x)$ (solid curve) compared with the static force A_1 .

We now discuss two successful applications of our VM approximation scheme.

(a) *dc bias*, $\Omega_1 = 0$, $\phi_1 = 0$. We consider first the case when the slow varying modulation embedded in $F(t)$ can be assimilated to a constant A_1 —at least over the relevant experimental observation times. The simplest choice for the substrate potential is

$$V(x) = -\cos x, \quad (12)$$

corresponding to setting $a_1 = -1$ and all the remaining Fourier coefficients a_n, b_n to zero. The reduced problem (9), (10) describes the Brownian diffusion in a washboard potential with variable tilt A_1 [20].

The observable that best quantifies the response of such a system to the dc input A_1 is the mobility $\mu \equiv \langle \dot{x} \rangle / A_1$. In figure 4 we compare the simulation data for the full dynamics (1)–(3) against the analytic predictions for the static limit of the LE (9), (10) (i.e. when $\Omega_1 = 0$, $\phi_1 = 0$) at increasing ratios A_2/Ω_2 of the ac component of $F(t)$. The solid curves displayed have been obtained by computing the analytic expression (11.51) of [20] for μ . The agreement between simulation and theory is surprisingly close even for noise intensities above our threshold of confidence (11).

(b) *Vibrational ratchets*. We consider now a more complicated example that falls under the category of rocked ratchets [21]. The motion of a Brownian particle on an asymmetric substrate gets rectified when driven by a time-correlated force, either of stochastic or of deterministic time-periodic origin [6]. Let the Fourier coefficients of the expansion (3) all be zero but $b_1 = -1$ and $b_2 = -\frac{1}{4}$, i.e.

$$V(x) = -\sin x - \frac{1}{4} \sin 2x. \quad (13)$$

The corresponding LE (1) describes a doubly-rocked ratchet [10, 11]. For arbitrary input frequencies Ω_1, Ω_2 , the rectified current of the system is known to exhibit marked

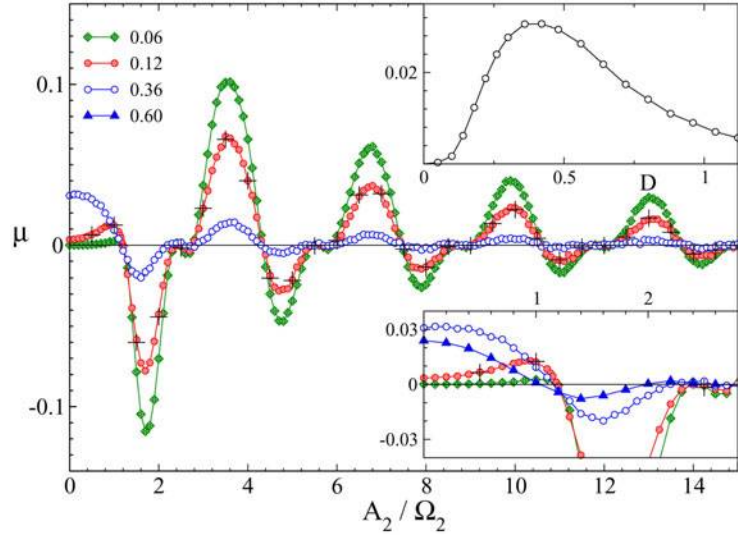


Figure 5. Mobility versus A_2/Ω_2 for the doubly-rocked ratchet (1) and (13) with $A_1 = 0.5$, $\Omega_1 = 0.01$, $\phi_1 = \phi_2 = 0$, and different values of the noise intensity D . All simulation data have been obtained for $\Omega_2 = 10$, with the exception of the black crosses, where we set $D = 0.12$ and $\Omega_2 = 20$. Bottom inset: simulation data for $\mu(A_2/\Omega_2)$ as in the main panel with an additional curve at $D = 0.6$. Top inset: μ versus D for $A_2 = 0$, $A_1 = 0.5$, and $\Omega_1 = 0.01$; circles: simulation data; solid curve: adiabatic formula (11.44) of [20].

commensuration effects and a complicated dependence on the noise intensity and all forcing parameters [11]. We claim here that an adiabatic limit exists for $\Omega_1 \rightarrow 0$ and $\Omega_2 \rightarrow \infty$ with A_2/Ω_2 constant, that can be well interpreted in terms of the separation scheme (7). Following the notation of [15, 16], we term a rocked ratchet operated under such conditions a *vibrational* ratchet.

The results of our simulation work are summarized in figures 5 and 6. To explain the persistent VM oscillations of the curves $\mu(A_2/\Omega_2)$, we write down the renormalized potential explicitly, i.e.

$$V(x) = -J_0(\psi_0) \sin x - \frac{1}{4} J_0(2\psi_0) \sin 2x. \quad (14)$$

As long as our adiabatic elimination procedure applies, the ratchet current $j = \langle \dot{x} \rangle / L$ vanishes in correspondence of the zeros of either Bessel function in equation (14), due to the restored symmetry of the effective substrate. On denoting by j_n the n th zero of $J_0(x)$, one predicts the following sequence of mobility-zeros:

$$\frac{A_2}{\Omega_2} = \frac{1}{2} j_1, j_1, \frac{1}{2} j_2, j_2, \frac{1}{2} j_3, j_3, \frac{1}{2} j_4, j_4, \frac{1}{2} j_5, j_5, \dots \quad (15)$$

with $j_1 = 2.405$, $j_2 = 5.520$, $j_3 = 8.654$, $j_4 = 11.79$, $j_5 = 14.93$, etc [18].

As shown in figure 5, the sequence (15) reproduces very closely the zero-crossings of our simulation curves for small noise intensities; for $D = 0.06$ we could locate correctly over 20 zeros of the curve $\mu(A_2/\Omega_2)$. In our derivation of the effective potential (14) we cautioned that discrepancies may occur for D above the confidence threshold (11); the deviations observed in the bottom inset of figure 5 invalidate our approximation scheme only for $D \gtrsim 1$. The amplitudes of the large $\mu(A_2/\Omega_2)$ oscillations decay like $(A_2/\Omega_2)^{-\frac{1}{2}}$ as expected after noticing that the modulus of $J_0(x)$ vanishes asymptotically like $\sqrt{2/\pi x}$ for $x \rightarrow \infty$ [18].

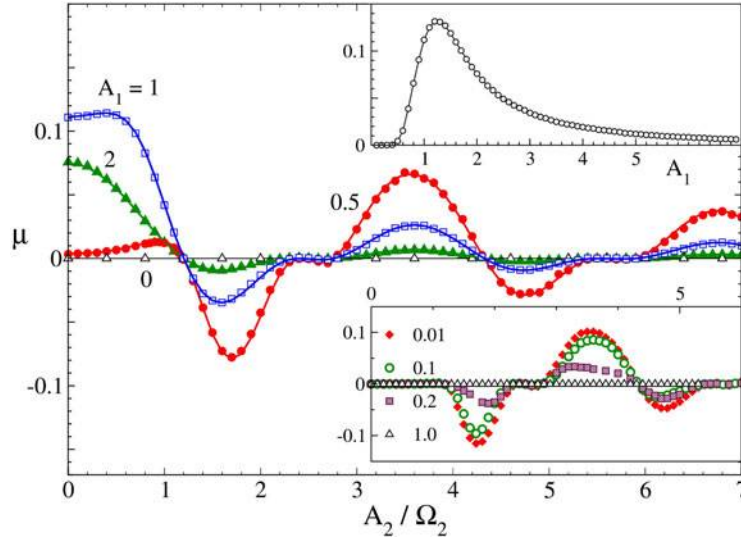


Figure 6. The mobility is depicted versus A_2/Ω_2 for the doubly-rocked ratchet (1) and (13) with $D = 0.12$, $\Omega_1 = 0.01$, $\Omega_2 = 10$, $\phi_1 = \phi_2 = 0$, and different values of A_1 . Top inset: μ versus A_1 for $A_2 = 0$, $D = 0.12$, and $\Omega_1 = 0.01$; circles: simulation; solid curves: adiabatic approximation (11.44) of [20]. Bottom inset: μ versus A_2/Ω_2 for the doubly-rocked ratchet (1) and (13) with $A_1 = 0.5$, $D = 0.12$, $\Omega_2 = 10$, $\phi_1 = \phi_2 = 0$, and different Ω_1 .

In the low-frequency regime, $\Omega_1 \ll 1$, the reduced ratchet dynamics, (9) and (14), can be treated adiabatically. Its mobility can be computed analytically by the time averaging equation (11.44) of [20] over one forcing cycle $t_1 = 2\pi/\Omega_1$. In figure 6 the analytic curves for $\mu(A_2/\Omega_2)$ fit our simulation data (grey dots) very closely at low noise, regardless of the value of the amplitude A_1 of the slow harmonic in (2). In the bottom inset of figure 6, deviations from the low-frequency curve become visible for $\Omega_1 \gtrsim 0.1$: this does not imply that the projection scheme leading to the reduced LE (9), (10) fails on increasing Ω_1 with $\Omega_1 \ll \Omega_2$, but rather that the adiabatic treatment of the resulting LE becomes untenable. This conclusion is corroborated by the fact that the mobility zeros (and signs) of the curves both in the main panel and in the bottom inset of figure 6 are independent of either parameter A_1 and Ω_1 of the low-frequency sinusoid.

4. Conclusions

In this preliminary report we numerically investigated the transport of an overdamped Brownian particle driven by a bi-harmonic force in two different frequency regimes, termed harmonic and vibrational mixing, respectively.

We compared the output of an extensive simulation project with the results of perturbation studies available in the literature. The emerging picture is encouraging for the VM regime, where a simple adiabatic scheme seems to reproduce our numerical data closely. Regarding the HM regime, however, the current analytical predictions are not yet quantitatively dependable.

We confirm that bi-harmonic drives do indeed play a prominent role in the physics of ratchets [10, 11]. In view of technological applications, we stress here a peculiar property of vibrational ratchets. As depicted in figure 6, in the presence of the high-frequency harmonic,

alone, $A_1 = 0$ and $\Omega_2 \gg 1$, the simulated net current is vanishingly small (empty triangles in the main panel); in the absence of fast oscillations, $A_2 = 0$, however, the curve $\mu(0)$ versus A_1 is well reproduced by the adiabatic limit $\Omega_1 \ll 1$ [21] (figure 6, top inset). On comparison, one notices that, for relatively small A_1 , the amplitude of the $\mu(A_2/\Omega_2)$ oscillations can grow notably larger than the corresponding $\mu(0)$. This means that energy pumped into the system at too high frequency gets dissipated into the heat bath, if the system is operated at equilibrium; in contrast VM induces a cooperative coupling between high-frequency disturbances and optimal drives, thus enhancing the system response beyond the expectations of the linear response theory.

On the other hand, the robustness of VM hints at the possibility of implementing this concept in the design and operation of efficient electromagnetic wave sensors. In fact, the present investigation has been inspired by a typical signal detection problem, namely how to reveal a high-frequency signal by means of a sensor with optimal sensitivity in a relatively low-frequency band. Our results suggest a simple recipe: although the unknown high-frequency signal alone cannot be detected, adding a tunable control signal with parameters within the device sensitivity range causes a nonlinear transfer of energy (information) from high to low frequencies, thus enhancing/modulating the sensor response to the control signal. By analysing the dependence of the device output on the tunable input signal, we can reveal the existence of unknown (and otherwise not detectable) high-frequency signals.

References

- [1] Seeger K and Maurer W 1978 *Solid State Commun.* **27** 603
- [2] Borromeo M and Marchesoni F 2004 *Europhys. Lett.* **68** 783
Borromeo M and Marchesoni F 2005 *Phys. Rev. E* **71** 031105
- [3] Wonneberger W and Breymayer H J 1981 *Z. Phys. B* **43** 329
- [4] Marchesoni F 1986 *Phys. Lett. A* **119** 221
- [5] Goychuk I and Hänggi P 1998 *Europhys. Lett.* **43** 503
- [6] Reimann P 2002 *Phys. Rep.* **361** 57
Astumian R D and Hänggi P 2002 *Phys. Today* **55** (11) 33
Hänggi P, Marchesoni F and Nori F 2005 *Ann. Phys., Lpz.* **14** 51
- [7] Luczka J, Bartussek R and Hänggi P 1995 *Europhys. Lett.* **31** 431
- [8] Flach S, Yevtushenko O and Zolotaryuk Y 2000 *Phys. Rev. Lett.* **84** 2358
Denisov S and Flach S 2001 *Phys. Rev. E* **64** 056236
- [9] Denisov S, Klafter J, Urbach M and Flach S 2002 *Physica D* **170** 131
Denisov S, Klafter J and Urbach M 2002 *Phys. Rev. E* **66** 046203
- [10] Savel'ev S, Marchesoni F and Nori F 2003 *Phys. Rev. Lett.* **91** 010601
Savel'ev S, Marchesoni F and Nori F 2004 *Phys. Rev. Lett.* **92** 160602
- [11] Savel'ev S, Marchesoni F, Hänggi P and Nori F 2004 *Europhys. Lett.* **67** 179
Savel'ev S, Marchesoni F, Hänggi P and Nori F 2004 *Phys. Rev. E* **70** 066109
Savel'ev S, Marchesoni F, Hänggi P and Nori F 2004 *Eur. Phys. J. B* **40** 403
- [12] Morales-Molina L, Quintero N R, Mertens F G and Sánchez A 2003 *Phys. Rev. Lett.* **91** 234102
Sukstanskii A L and Primak K I 1995 *Phys. Rev. Lett.* **75** 3029
Kivshar Yu S and Sánchez A 1996 *Phys. Rev. Lett.* **77** 582
Salerno M and Zolotaryuk Y 2002 *Phys. Rev. E* **65** 056603
Marchesoni F 1996 *Phys. Rev. Lett.* **77** 2364
Ustinov A V *et al* 2004 *Phys. Rev. Lett.* **93** 087001
- [13] Borromeo M, Costantini G and Marchesoni F 2002 *Phys. Rev. E* **65** 041110
- [14] Bleckman I I 2000 *Vibrational Mechanics* (Singapore: World Scientific)
- [15] Landa P S and McClintock P V E 2000 *J. Phys. A: Math. Gen.* **33** L433
- [16] Zaikin A A *et al* 2002 *Phys. Rev. E* **66** 011106
Baltanás J P *et al* 2003 *Phys. Rev. E* **67** 06611
Ullner E *et al* 2003 *Phys. Lett. A* **312** 348

- Casado-Pascual J and Baltanás J P 2004 *Phys. Rev. E* **69** 046108
Casado-Pascual J and Baltanás J P 2004 *Phys. Rev. E* **69** 059902 (Publishers note)
- [17] Borromeo M and Marchesoni F 2005 submitted
 - [18] Abramowitz M and Stegun I 1972 *Handbook of Mathematical Functions* (New York: Dover)
 - [19] Marchesoni F and Grigolini P 1983 *Physica A* **121** 269
Marchesoni F and Grigolini P 1984 *Z. Phys. B* **55** 257
 - [20] Risken H 1984 *The Fokker–Planck Equation* (Berlin: Springer) chapter 11
 - [21] Bartussek R, Hänggi P and Kissner J P 1994 *Europhys. Lett.* **28** 459